IEEE Access
Multidisciplinary | Rapid Review | Open Access Journal

Received 1 November 2023, accepted 28 November 2023, date of publication 5 December 2023,
date of current version 12 December 2023.

Digital Object Identifier 10.1109/ACCESS.2023.3339615

RESEARCH ARTICLE

A Metasurface-Based Electronically Reconfigurable and Dual-Polarized Reflectarray Antenna for Beam-Steering Applications

PUBET SANGMAHAMAD[1], PANUWAT JANPUGDEE[1,2], (Member, IEEE), AND YAN ZHAO[3], (Senior Member, IEEE)

[1]Department of Electrical Engineering, Faculty of Engineering, Chulalongkorn University, Bangkok 10330, Thailand
[2]Wireless Network and Future Internet Research Unit, Chulalongkorn University, Bangkok 10330, Thailand
[3]International School of Engineering, Faculty of Engineering, Chulalongkorn University, Bangkok 10330, Thailand

Corresponding author: Yan Zhao (yan.z@chula.ac.th)

This work was supported by the Thailand Science Research and Innovation Fund Chulalongkorn University under Grant CU_FRB65_ind (8)_156_21_22.

ABSTRACT In this work, a metasurface-based, 1-bit electronically reconfigurable reflectarray antenna (RRA) is proposed for dual-polarization beam-steering applications. The proposed RRA consists of 16 × 16 Jerusalem cross-shaped unit cells loaded with PIN diodes, which are used as active and reconfigurable devices to generate a reflection phase difference of 180° between their on- and off-states. An optimal focal length to diameter ratio (f/D) for the feed antenna is determined to maximize its radiation coverage on the RRA. Microcontroller-based shift registers are used to resolve the complexity of the individual DC bias networks for the PIN diodes. The proposed RRA is designed, fabricated, and measured to evaluate its beam-steering performance. The measurement results show that the proposed RRA can achieve beam-steering of ±60° for x- and y-polarizations in both azimuth and elevation planes. Moreover, the proposed RRA is further verified by full-wave simulations to evaluate its additional functions, such as the generation of sum and difference beams for monopulse radar systems. The proposed RRA is anticipated to have significant potential in areas such as wireless communications, imaging, and radar systems, and is a particularly suitable candidate for reconfigurable intelligent surfaces (RISs) due to its adaptability and capability of dynamically generating different radiation patterns.

INDEX TERMS Reconfigurable reflectarray antenna, reflective metasurface, beam-steering, PIN diode.

I. INTRODUCTION

Metamaterials (MTM) are engineered materials with extraordinary electromagnetic (EM) properties that cannot be found in naturally occurring materials such as negative refractive index. However, the initially proposed metamaterials suffer from their bulky size, low efficiency, and complex manufacturing process. On the other hand, ultra-thin metasurfaces (MTS), the two-dimensional counterpart of the MTM, have emerged as a more efficient and simpler alternative [1], [2]. More recently, reconfigurable metasurfaces (RMTs) have attracted a great deal of attention from researchers, due to their capability of actively manipulating EM waves to enhance system performance. This has led to the emerging of intriguing meta-devices and exploration of exotic physical phenomena, and enabling applications such as beam control and focusing lenses [3]. The versatility and potential of the RMTs drive innovative research in various fields, and has led to the study and development of reconfigurable reflectarray antennas (RRAs) [4], [5], [6], [7], [8], [9], [10], [11], [12], [13], [14], [15], [16], [17], [18]. The RRAs combine the advantages of both parabolic reflectors and microstrip array antennas to overcome their limitations. Parabolic reflectors are costly and lack wide-angle beam

The associate editor coordinating the review of this manuscript and approving it for publication was Wanchen Yang.

scanning, while microstrip arrays require expensive phase shifters and suffer from energy loss. The RRAs offer low-cost and wide-angle beam-steering capabilities by using meta elements/unit cells arranged in a planar array to form a large metasurface, functioning similarly to a parabolic reflector. The feeding antenna illuminates EM waves on the RRA, which are then reflected to the desired directions or angles.

In the unit cell design, the reflection phase can be changed by adjusting certain parameters. The passive unit cell of reflectarrays (RAs) achieves this through different techniques, namely, size variation, delay line length change, unit cell rotation, or subwavelength periodicity variation [19]. However, their fixed geometry limits their tunability. The RRAs overcome this limitation and enable dynamic EM wave manipulations. Different tuning mechanisms, such as mechanical movement [14], [15], MEMS [16], liquid crystal [17], [18], varactor diodes [13], and PIN diodes [4], [5], [6], [7], [8], [9], [10], [11], [12] provide reconfigurability by changing the unit cell's reflection phase [20]. Mechanical RRAs utilize servos, micro motors, or similar equipment to change the unit cell's EM responses. It offers high linearity, but slower responses compared to electrical systems. Electrical RRAs use MEMS switches, providing fast and precise beam steering with a wide dynamic range. However, their designs are complex and expensive. Liquid crystal is a type of material in between solid and liquid states, and adjusting voltage can alter its permittivity to introduce phase differences. But it has the limitations of being expensive and slow in response. Alternatively, RRA unit cells can be represented by RLC circuits, and their EM response is controlled by adjusting the RLC parameters. Varactor diodes and PIN diodes can be also embedded to electronically adjust RRA properties. Varactor diodes change capacitance with voltage, allowing phase adjustment and beam-steering. However, they have limited dynamic range, high power consumption, and complexity in designing voltage-controlled circuits. In contrast, PIN diodes are widely used in RRAs [4], [5], [6], [7], [8], [9], [10], [11], [12], and reflection phase can be modified through the change in resistance, capacitance, and inductance with applied DC voltage. PIN diodes offer low power consumption and low insertion loss compared to varactor diodes, as well as simplicity and cost-effectiveness. Switching the PIN diodes on or off with different DC voltages can achieve a 180° reflection phase change, making them suitable for 1-bit programmable RRA. Programmable controllers such as field-programmable gate arrays (FPGAs) [10], [21] and microcontroller units (MCUs) [5], [6], [12], [13], [22], [23] are used to achieve programmability in RRA. These controllers not only respond to external stimuli, but also bridge EM characteristics and digital information systems, enabling communication and coordination between the physical world and the digital domain.

Recently, RRAs have generated substantial research interests, with several reported works focusing on single-polarized RRAs [5], [6], [7], [8], [9], [13]. Works in [6] and [7] present single-band, single-polarized 1-bit RRAs operating at 5.8 GHz and 9.85 GHz. A dual-band, single-polarized RRA is demonstrated in [9], utilizing a rectangular patch with a PIN diode. While capable of beam-steering at two frequencies, this RRA lacks independent dual-band beam-steering. Additionally, wideband single-polarized RRAs have been demonstrated in other works [5], [8], [13]. The RRA in [13] utilizes varactor diodes for continuous phase tuning, achieving ±55° beam-steering. However, its unit cell control is not independent due to the column control for varactor diodes. For independently controlled unit cells, loaded PIN diodes are used in RRAs presented in [5] and [8], achieving ±60° and ±55° beam-steering performance, respectively. Traditionally, achieving dual polarization beam-steering often requires complex and bulky systems, such as dual-feed antennas or separate phased arrays for each polarization. The RRA provides a compact and efficient solution for dual-polarized beam-steering, eliminating the need for complex and bulky systems. Its unit cells incorporate electronically switchable devices, enabling independent control of reflection properties for both polarizations. This allows the RRA to create independent and steerable beams in desired directions with different polarizations [24], [25], [26], [27]. In [24], the authors present a 1-bit dual-band and dual-polarized RRA with a rectangular patch containing two PIN diodes per unit cell for beam-steering. This RRA achieves two-dimensional beam scanning of up to ±60°. However, it is designed with fixed frequencies for each polarization control (12.5 GHz for x-polarization and 14.25 GHz for y-polarization). Moreover, it requires a complex RF circuit chain to generate dual frequencies. This RRA lacks the ability to perform polarization synthesis, limiting its capability to generate arbitrary linear and circular polarizations. Two recently published papers have presented single-band and dual-polarized RRAs [25], [26]. In [25], a dual-polarized RRA operating at 7.45 GHz is implemented, with each unit cell containing four PIN diodes. However, this RRA exhibits lower aperture efficiency compared to other RRAs [24], [26], possibly due to excessive PIN diode usage causing element losses. In [26], the authors propose an RRA with a symmetrically rotated sub-array for dual-polarized beam-steering at 10 GHz. This work achieves ±60° beam-steering with ±20° increment for both polarizations and in both E- and H-planes. Each sub-array consists of four-unit cells, two for each polarization, with a symmetrically rotated configuration. However, the added spacing between adjacent and same polarized unit cells can complicate the minimization of spacing losses.

In this work, we focus on the design, simulation, fabrication, and measurement of an RRA specifically tailored for independent and simultaneous dual-polarization and wide-angle beam-steering. By exploring the unique advantages of the proposed metasurface-based RRA formed by novel Jerusalem cross-shaped unit cells loaded with PIN diodes, we aim to contribute to the advancement of beam-steering technology and demonstrate a further application of the proposed RRA in order to produce sum and difference

beams in monopulse radar systems. The rest of this article is organized as follows. Section II presents the electronically RRA design, which describes the unit cell, DC biasing, control board design, and prototype fabrication. Section III introduces the overall system design of the proposed RRA. Simulation and measurement results of the proposed RRA and conclusions are provided in Section IV and Section V, respectively.

II. DESIGN OF THE RRA

In order to realize the proposed independent and simultaneous dual-polarizations and wide-angle beam-steering using a metasurface-based electronically reconfigurable reflectarray antenna (RRA), the metasurface's unit cell for independent control of the reflection phase for orthogonal polarizations with a minimum effect to each other should be designed. Thanks to the geometry of Jerusalem cross-shaped structure, the resonant frequency can be tuned by varying the length of each arm. Therefore, to achieve the proposed electronically RRA for dual- polarizations and wide-angle beam scanning, in this work, the Jerusalem cross-shaped structure has been designed with PIN diodes loaded on both orthogonal arms. The design of the proposed electronically RRA for dual-polarizations can be separated into three sub-sections, Sub-section A: the unit cell design, Sub-section B: the DC bias and control boards design, and Sub-section C: the prototype fabrication.

A. UNIT CELL DESIGN

The unit cell structure of the proposed 1-bit dual-polarized reconfigurable metasurface is shown in Figure 1. The dimensions of the unit cell are $0.29\lambda_0 \times 0.29\lambda_0$ where λ_0 is the wavelength at the operating frequency of 5.8 GHz. The top layer has a Jerusalem cross-shaped structure, and the bottom layer is a full metallic ground, connected to the top layer by three vias for grounding and biasing purposes, as illustrated in Figure 1. Two neighboring arms of the Jerusalem cross are loaded with PIN diodes in the gap between the arm and the central metallic structure of the top layer, with each PIN diode serving to control one polarization. The PIN diode is electronically switched to on-state or off-state according to the direct current (DC) biasing voltage through the biasing via, which generates a certain phase difference between each PIN diode state. The central metallic via is connected to the ground layer as a negative biasing electrode. Meanwhile, another two metallic vias are connected from the top layer through the substrate layer, to the biasing layer as positive biasing electrodes. Two metallic ground holes with larger radii than the metallic vias are etched on the corresponding positions of the ground metallic layer to achieve DC isolation between the positive and negative biasing electrodes. The substrate used is Roger RT5880 with a thickness of 3.175 mm, and relative dielectric constant (ε_r) and loss tangent ($tan\delta$) of 2.2 and 0.0009, respectively.

For the PIN diode model, a low-insertion loss type, SMPA 1320-079LF is used as the active components, which covers

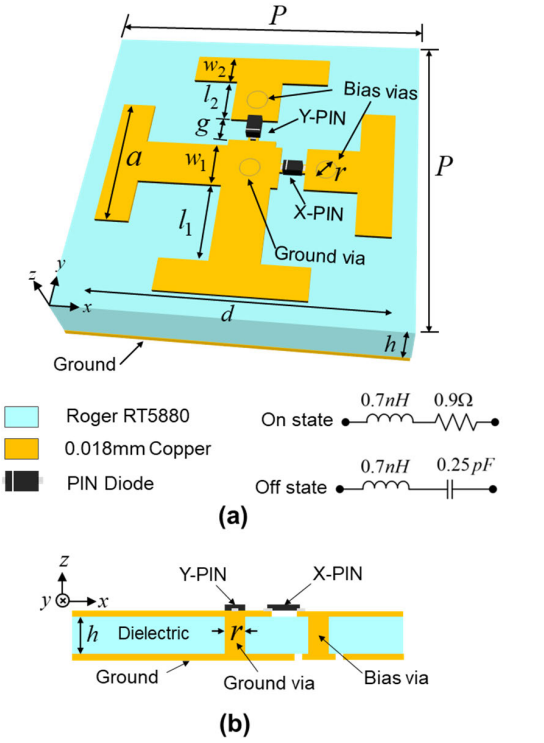

FIGURE 1. Structure and dimensions of the unit cell. (a) A 3D view of the unit cell and the equivalent circuit parameters of the PIN diode model SMPA 1320-079LF. (b) Side view of the unit cell.

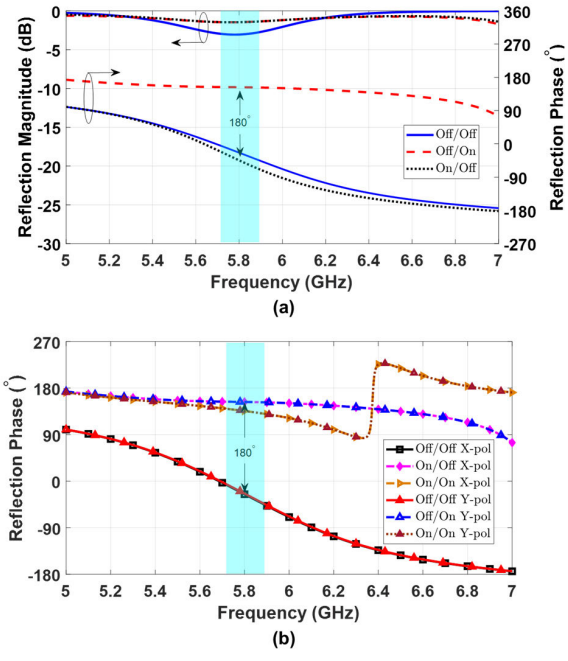

FIGURE 2. Frequency responses of the proposed unit cell for normal incidence from simulations. (a) Reflection magnitudes and phases for *y*-polarized incidence. (b) Phase response for *x*- and *y*-polarized incidences.

the desired frequency band. The model of the PIN diode is selected based on its features of high efficiency and

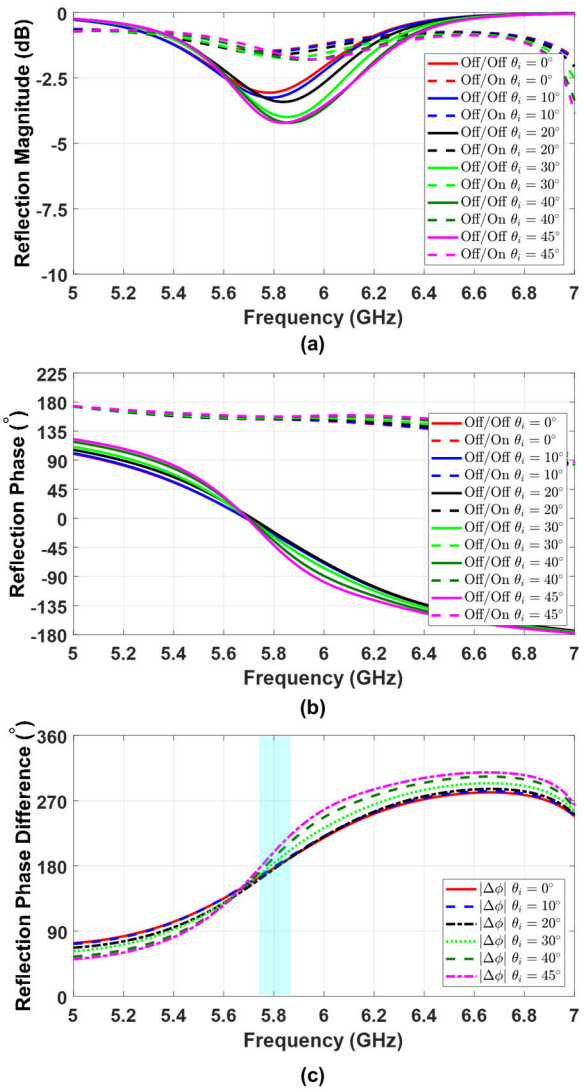

FIGURE 3. Frequency responses of the proposed unit cell for oblique incidences from simulations. (a) Reflection magnitude. (b) Reflection phase. (c) Reflection phase difference between two PIN diode states.

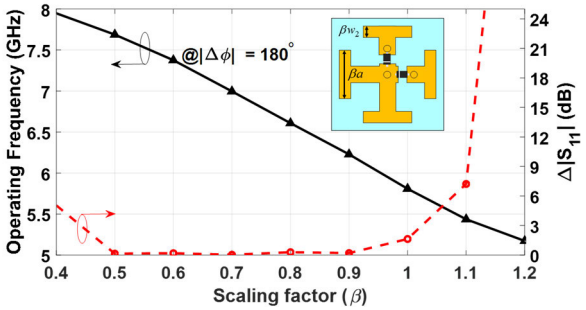

FIGURE 4. The operating frequency as a function of the scaling factor β, and the difference in reflection magnitude ($\Delta|S_{11}|$) at the corresponding operating frequency.

programmability. For the on-state, the PIN diode is modeled as a lumped resistance (R) of 0.9 Ω connected in series with a lumped inductance (L) of 0.7 nH. On the other hand, for the off-state, it can be represented by a lumped capacitance (C) of 0.25 pF connected in series with a lumped inductance of 0.7 nH. In numerical simulations, the "on" and "off" states of the PIN diode are represented by equivalent circuits shown in Figure 1(a). The optimized parameters of the final unit cell design shown in Figure are given as follows (unit: mm): $P = 15$, $d = 13.1$, $a = 6$, $g = 1.5$, $l_1 = 2.9$, $l_2 = 1.2$, $w_1 = 2.2$, $w_2 = 2.55$, $r = 0.7$, and $h = 3.175$. A commercial electromagnetic simulation software CST Microwave Studio (CST MWS) is used to analyze and optimize the proposed unit cell. To account for the interactions between neighboring unit cells in the full metasurface, the unit-cell boundary condition and two Floquet ports along the z-axis are applied, and the simulation frequency ranges from 5 to 7 GHz. The simulated reflection magnitude and phase for y-polarized excitation on the unit cell are plotted in Figure 2(a).

It is clearly observed that at 5.8 GHz, the difference in reflection phase ($|\Delta\phi|$) between the off/off and off/on modes is around 180°, and reflection magnitudes are higher than −3 dB. Here, the PIN diode states before and after the slashes (/) represent the coding PIN diode states along the x-direction (X-PIN) and y-direction (Y-PIN), respectively. The light blue area shows the phase bandwidth of the 1-bit reconfigurable coding metasurface unit cell as the phase difference satisfies an acceptable range of 180° ± 20° between the two coding states [8], [28]. More significantly, only the working states of PIN diodes connected in the parallel direction influence the reflection response of the unit cell, and those connected in the orthogonal direction have no effect. As shown in Figure 2(a), under y-polarized excitation, the status of off/off and on/off (varying the X-PIN diode state) shows little difference in the reflection phase response (less than 20°) [8], [28]. After changing the working states of the Y-PIN diode from off/off and on/off to off/on, a 180° reflection phase is obtained. It indicates the low mutual coupling between two orthogonal polarizations of the proposed unit cell. These results demonstrate that the proposed unit cell meets the requirement of our design. In addition, the on state is regarded as "1" and the off state is "0" of the PIN diode programmable coding state. Figure 2(b) shows the comparison of reflection phase between the x-polarized and y-polarized incident waves. It can be seen that the reflection phase is not significantly affected by the incident wave's polarizations.

When oblique incidence occurs on a unit cell, its performance may be affected. Thus additionally, we study the unit cell's performance under oblique incidence. The investigation on the effect of oblique incidence on the unit cell is only carried out for the y-polarized wave due to the structure's symmetry, and identical findings may be achieved for the x-polarization. It is shown that the unit cell achieves steady phase performance when the EM wave impinges at angles of 10°, 20°, and 30°, as illustrated in Figure 3. In Figures 3(b) and 3(c), even at 40° and 45° of oblique incidence, the phase difference could be controlled within an acceptable range of ±20°. Particularly at the 5.8 GHz

frequency, the phase difference is only 198° for the incident angle of 45°. The unit cell's optimal performance guarantees the performance of the proposed RRA. Furthermore, when the incident angle is larger, the reflection magnitude is slightly reduced, as shown in Figure 3(a). Because more incoming waves illuminate at the edge of the unit cell. Whereas in the 45° of incident angle, the difference in reflection magnitude between two PIN diode states is less than 3 dB.

Another advantage of the proposed unit cell is the ease of modifying the operating frequency by adjusting the width (w_2) and length (a) of the cross-shaped arms. A scaling factor (β) is used to conveniently scale both width and length simultaneously. Simulation results in Figure 4 show that varying β from 0.4 to 1.2 decreases the operating frequency from 7.95 to 5.14 GHz when considering $|\Delta\phi|$ as 180°. The relationship between β and frequency is quite linear, with a slope of -3.6. Additionally, $\Delta\,|S_{11}|$ (the difference in reflection magnitude) between two states at each frequency concerning β is less than -3 dB when β is between 0.5 and 1, and the frequency is in the range of 7.68 to 5.8 GHz (see Figure 4, red dashed line).

B. DC BIAS AND CONTROL BOARDS DESIGN

The proposed RRA consists of three main boards: a 16 × 16 unit cells reflective metasurface, a DC biasing board, and a programmable control board. The circuit diagram of the connections between these three boards is shown in Figure 5. Both DC bias and control boards are fabricated using FR-4 substrates with 0.8 mm in thickness. The top board is the proposed reflective metasurface which is composed of 256 unit cells arranged in a planar array with a total size of 240 × 240 mm^2. The second layer is a DC biasing board which is used for independently connecting each PIN diode and the control board. The DC biasing board is placed closely behind the reflective metasurface and directly and individually connected to PIN diodes via small metallic pins of 0.5 mm in diameter. Three of the bias points from the reflective metasurface's unit cell (two for PIN diode positive biasing pins and one for ground) are connected to the biasing board through metallic vias. In the DC biasing network, the use of high-frequency series inductors and parallel capacitors can create a low-pass filter to suppress radio frequency (RF) signals. This approach ensures good isolation between the DC and RF signals, preventing any interference or coupling between them. The design of the biasing board is shown in Figure 6(a). Sixteen connectors are placed on both sides of the biasing board for the direct connection to the control board via ribbon cables. The overall size is 327 × 258 mm^2.

The third board is a programmable control board. To reduce the complexity of wiring and the MCU host system, 64 shift registers (32 for each polarization) of model 74HC595D are utilized to control 512 PIN diodes sequentially. It is important to note that each PIN diode is connected in series with an LED to show the PIN diode's state. Green LEDs indicate the states of X-PIN diodes, while red LEDs represent Y-PIN diodes' states. Thirty-two sockets are equally separated into two groups and placed at the position of the left and right edges of the board for the connection with the DC biasing board. The control board utilizes a low-cost, dual-core Arm Cortex M0+ processor RP2040, which operates at a system clock speed up to 133 MHz, with 264 kB of SRAM, and 2 MB of flash memory, which can meet the demand of real-time signal processing. The design of the control board based on shift registers is shown in Figure 6(b) with an overall size of 400 × 240 mm^2.

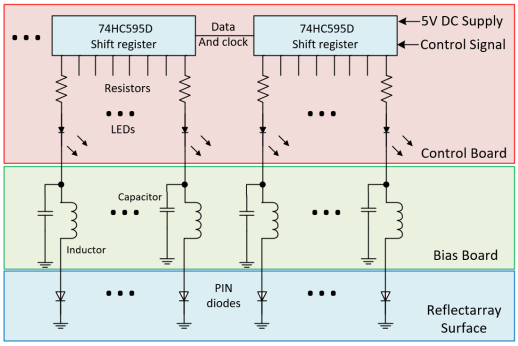

FIGURE 5. The circuit diagram of the proposed RRA.

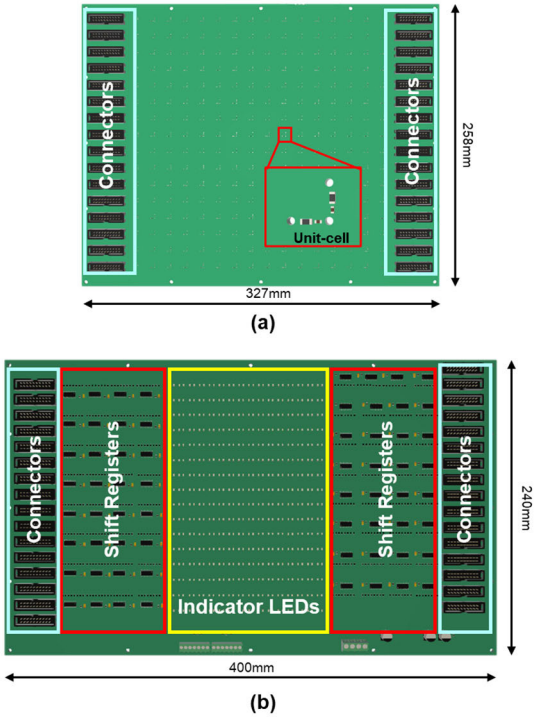

FIGURE 6. The layouts of (a) the DC bias board and (b) the control board based-on shift registers.

C. PROTOTYPE FABRICATION

To validate the design principle and simulation results, the RRA prototype, an independent PIN diode's biasing

board, and a control board are fabricated through the standard printed circuit board (PCB) technique, as shown in Figures 7(a) and 7(b) for the components setup and the photograph of the prototype, respectively. The RRA consists of 16 × 16 unit cells reflective metasurface combined with 512 PIN diodes (2 PIN diodes/unit cell), the unit cell is proposed and described in Section II-A, arranged to form a square planar array with dimensions of D along the x- and y-axes. The proposed RRA has an effective size of 240 × 240 mm^2. PIN diodes are soldered on the unit cell's front metal layer with a common cathode connected to the unit cell's center and linked to the biasing ground. The DC biasing board is installed as closely as possible behind the RRA, with their backsides facing each other. It should be noticed that the biasing board is positioned behind the ground plane of the reflective metasurface to ensure that the biasing line has no effect on reflected waves. To control each PIN diode separately, a direct connection is established between each DC biasing line and its particular PIN diode via metallic pins. Subsequently, each PIN diode is connected in series with an LED and a resistor on the control board. This setup not only indicates the state of the PIN diode but also proposes current limitation. Following that, biasing lines are connected to the output pin of the shift register. For alignment and stability, 3 mm diameter nylon bolts and nuts and 3D-printed supports are employed. Furthermore, the biasing board is linked to the control board through 32 ribbon cables. The control board is likewise positioned and secured using the same method as the biasing board. A WR159 standard open-ended waveguide is used as the feeding antenna, with the supporting structure printed by a 3D printer to avoid assembly alignment errors. The feeding antenna is placed at the center of the RRA at an optimum focal distance on the z-axis.

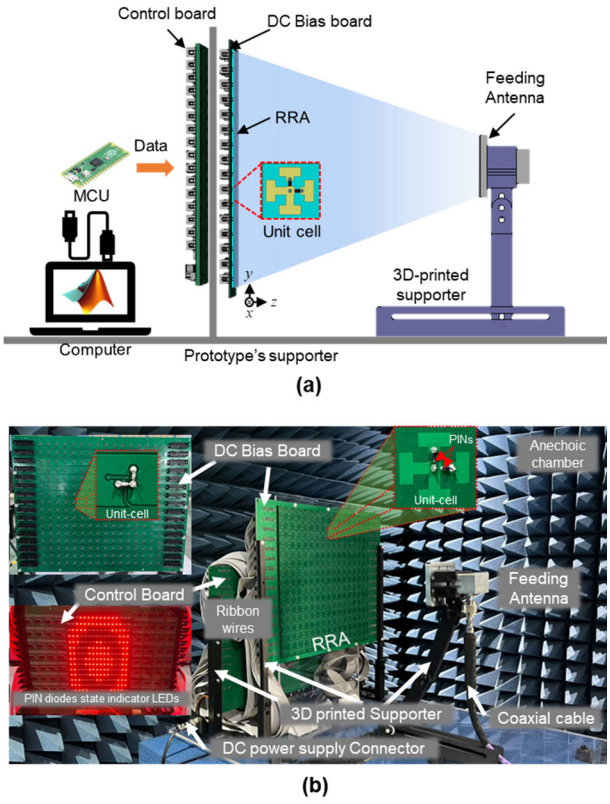

FIGURE 7. The components of the proposed RRA. (a) The diagram showing all components. (b) The photo of the actual RRA prototype.

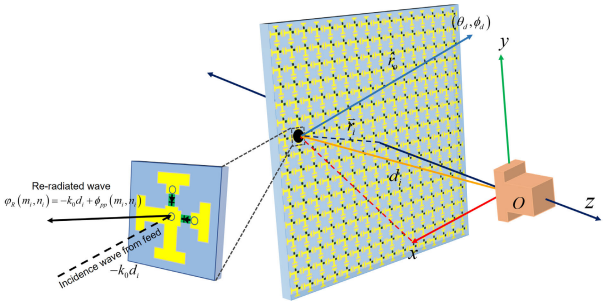

FIGURE 8. Geometry of the RRA and the direction of the re-radiated wave on the unit cell.

III. THE OVERALL RRA SYSTEM DESIGN

In this section, the whole structure of the proposed RRA with 16 × 16 unit cells is analyzed in terms of the feeding antenna distance and the calculation of phase distribution patterns. Each part is described in detail below.

A. SELECTION OF THE FEEDING LOCATION

In order to illuminate the RRA with a spherical wave feeding antenna, the distance between the center of the RRA's aperture and the center phase of the feeding antenna, known as the focal distance (f), needs to be determined to maximize the gain and efficiency of the RRA. The spillover and illumination losses are the two key contributors to the RRA losses [29]. If the feeding antenna is too far away from the RRA, a portion of the incident waves will be lost by going beyond the RRA's boundaries; this squandered energy is known as the spillover loss. On the other hand, when the feeding antenna is placed too close to the RRA, a portion of the RRA will remain unilluminated, resulting in the illumination loss. Therefore, to increase antenna efficiency, the optimum feeding antenna location should be optimized. The total efficiency of the RRA antenna is the product of spillover efficiency (n_S) and illumination taper efficiency (n_I) [29]. The gain of the RRA antenna is also significantly influenced by the feed's position, known as the focal diameter ratio (f/D) where D is the length of the RRA. The feed radiation level at the RRA's edge will typically be set to −10 dB or −10 dB tapper which is normalized to the peak value of the feeding antenna radiation. In this work, a WR159 linearly polarized rectangular open-ended waveguide is adopted as the feeding antenna. The WR159 was constructed and simulated in CST MWS software. The dimensions and physical parameters of WR159 are extracted from the manufacturer's official datasheet. After that, simulations are performed and compared to the measurement results, in terms

of S-parameters, radiation patterns, and gains. Therefore, to maximize the aperture efficiency, the f/D is set to 0.5.

B. CALCULATION OF THE REQUIRED PHASES FOR RRA

The phase correction required for each unit cell is characterized by the distribution pattern of phase shifts. Typically, the distance of the feeding antenna to the unit cells has a direct impact on the phase difference. Specifically, as the distance between the feed and the unit cell increases, the phase difference relative to the nearest unit cell also increases. The unit cell that is at the closest distance to the feed phase center acts as the phase reference for the remaining unit cells. In this study, an analytical technique, as described in [19] and [30], is employed. Figure 8 shows the schematic geometry of the RRA and visualization of the re-radiated wave on the unit cell. The required unit cell's phase can be calculated by adding the spatial phase delay (ϕ_{sp}) which is a phase profile proportional to the distance from the feed phase center to the unit cell as given in (1):

$$\phi_{sp} = -k_0 d_i \tag{1}$$

$$k_0 = 2\pi/\lambda \tag{2}$$

where k_0 is the free space propagation constant and the negative sign comes from the $e^{j\omega t}$ convention and d_i is the distance from the phase center of the feed to the i^{th} unit cell. Then to produce a collimated beam in the designed spherical coordinate direction (θ_d, ϕ_d), a progressive phase (ϕ_{pp}) can be added to the RRA aperture in the form of (4):

$$\phi_{pp} = -k_0 \vec{r}_i \cdot \hat{r}_0 \tag{3}$$

$$\phi_{pp} = -k_0 \left(m_i sin\theta_d cos\phi_d + n_i sin\theta_d sin\phi_d\right) \tag{4}$$

Then, the required phase at each RRA's unit cell $\varphi_R(m_i, n_i)$ can be found by compensating for the spatial phase delay introduced by the feeding antenna expressed as of (5) and (6) [19], [30]:

$$\varphi_R(m_i, n_i) = \phi_{sp} - \phi_{pp} \tag{5}$$

$$\varphi_R(m_i, n_i) = k_0 \left[d_i - \left(m_i cos\phi_d + n_i sin\phi_d\right) sin\theta_d\right] \tag{6}$$

where (m_i, n_i) are the Cartesian coordinates in the x-y plane of the i^{th} unit cell. From the above equations, one may realize that the phase compensation might not lie within the range between 0 and 2π. Then, it should be shifted to the range of $[0, 2\pi]$ before being quantized. Considering a 1-bit coding unit cell, the quantized phase can be given as:

$$\phi_{quantized} = \begin{cases} 0, & \phi_{continuous} \in [0, \pi) \\ \pi, & \phi_{continuous} \in otherwise \end{cases} \tag{7}$$

where $\phi_{continuous}$ is the continuous phase distribution between $[0, 2\pi]$ which is defined from $mod(\varphi_R(m_i, n_i), 2\pi)$, where $mod(\cdot)$ is a modulo operation for required precise phase compensation divided by 2π. From $\phi_{quantized}$, the phase of 0 can be stated as a bit '0' or the 'off' state of the PIN diode. While the phase of π can be stated as a bit '1' or PIN diode's 'on' state. The phase distribution on the 16×16 unit cells RRA with designed parameters for boresight beam radiation under continuous phase $(\phi_{continuous})$ and 1-bit quantized phase $(\phi_{quantized})$ configurations are shown in Figures 9(a) and 9(b), respectively.

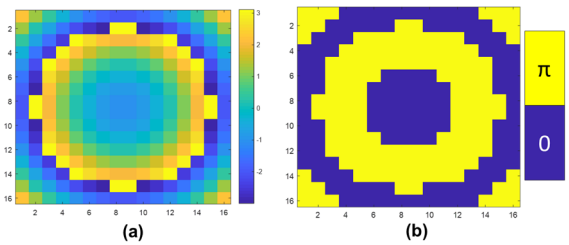

FIGURE 9. Phase distributions on the RRA for boresight beam radiation (a) Continuous phase before quantization. (b) After 1-bit quantization.

IV. SIMULATION AND EXPERIMENTAL RESULTS

A full structure of 16×16 unit cells RRA with an overall size of 240×240 mm^2 $(4.64 \times 4.64\lambda_0^2)$ is simulated with the WR159 open-ended rectangular waveguide located at the optimal focal distance of $0.5D$ as the feeding antenna. Simulations using CST MWS with open boundaries (add space) for all axes are performed. The center feed of the WR159 feeding antenna is placed in the center of the RRA in the x-y plane at a focal distance along the z-direction. In the simulation, to define the suitable lumped element of the PIN diode's state for each unit cell of the whole RRA, MATLAB is used to calculate the continuous phase distributions and quantized ones according to (6) and (7), respectively. Then the quantized phase of RRA from MATLAB is exported to the Visual Basic (VBA) macros script and used in simulations. The VBA macros are used for automatically defining PIN diode's lumped elements for 'on' and 'off' states, which aided to reduce the time and complexity for constructing the full RRA structure's simulation. The lumped element of the PIN diode is defined as a circuit model in Figure 1(a).

For evaluating the performance of the proposed RRA, measurement of the prototype has been conducted. The radiation pattern measurement setup and the photograph in an anechoic chamber are shown in Figures 10(a) and 10(b), respectively. The full structure of RRA, the programmable control board, and the feeding antenna are placed on a turntable. And when the turntable rotates, the feeding antenna is rotated accordingly to keep the same illumination angle to the RRA. The feeding antenna and the standard receiving horn antenna (Rx) are connected to a vector network analyzer (VNA) located outside the anechoic chamber via low-loss coaxial cables on port 1 and port 2, respectively. The short-open-load-through (SOLT) calibration method is used to calibrate the VNA to ensure the measurement accuracy. The center of the standard Rx horn antenna is placed at a distance of 2.5 meters from the center of the RRA. The measurement data are recorded by the VNA at a resolution of 0.2 degree during the turntable's rotation. The programmable control board is placed behind the RRA and connected to

the computer via a USB cable. The computer with MATLAB software is utilized to perform real-time calculations of phase distributions for the desired beam patterns. Then the data are directly sent to the control board for achieving beam-steering. A 5 V voltage source is used as the DC power supply for the control board, and it is placed on the floor behind the turntable to prevent wave reflections. During the measurement, the turntable rotates from −90° to 90° in the azimuth plane. While in the elevation plane, the turntable moves in a range of −35° and 35° due to the constraints in the prototype measurement setup.

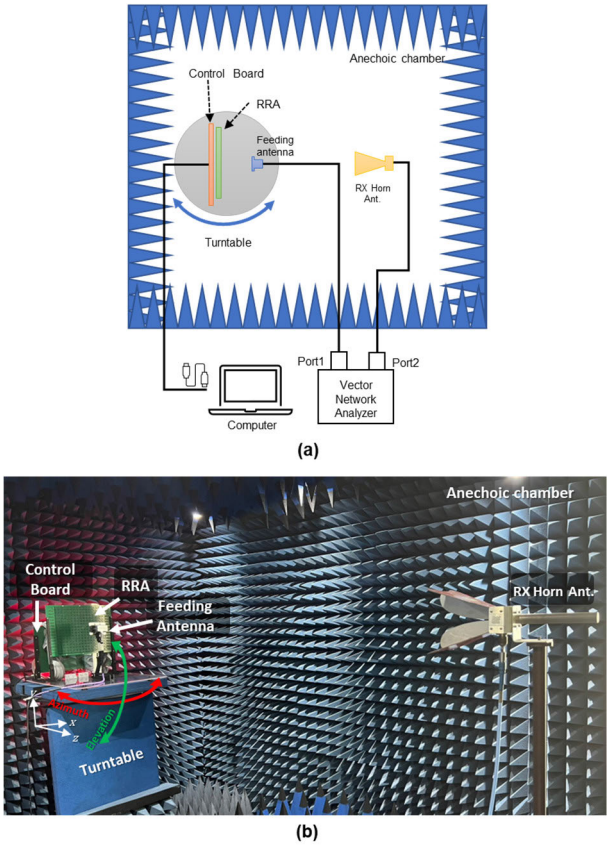

FIGURE 10. Measurement of the radiation pattern in an anechoic chamber. (a) The schematic diagram. (b) The photo of the measurement setup for the fabricated RRA prototype.

Figures 11(a) and 12(a) show the simulation and measurement beam-steering results of the proposed RRA operating under *x*-polarized excitations in the azimuth plane (*xoz*-plane). By adjusting the phase distributions of the RRA, wide-angle beam-steering is also attainable on the elevation plane (*yoz*-plane), as shown in Figures 11(b) and 12(b) for simulation and measurement results, respectively. By switching the unit cell's code of the RRA through programming, wide-angle beam-steering from −60° to 60° with a 10° step becomes observable. The ability of dynamically altering phase distributions allows for agile control of the radiation pattern, enabling beam-steering across a wide range of angles in both the azimuth and the elevation planes. Additionally, Figures 11(c), (d) and 12(c), (d) show the simulation and measurement results when *y*-polarized excitations incident on both observation planes. The measured beam-steering results in the elevation plane are restricted to a range of −35° to 35° due to the limited movement capabilities of the prototype setup on the turntable. The maximum beam point error in the simulation results for *x*-polarization is 2.8° and 2.6° in the azimuth and elevation planes at the beam-steering angles of −30° and −40°, respectively. The beam point error for *y*-polarization is 2.8° and 3.3° in the azimuth and elevation planes at the beam-steering angles of −40° and 30°, respectively. While for the measured results in the azimuth plane, the maximum beam point error is 4.4° at the angle of −40° under *x*-polarization. Additionally, in the elevation plane, for instance when the beam-steering directions are less than −20°, the radiation patterns exhibit anomalies, leading to errors in beam pointing and a decrease in gain. These anomalies are attributed to obstructions posed by the prototype supporter and the turntable. However, the agreement between measured and simulated results for other beam-steering directions is satisfactory.

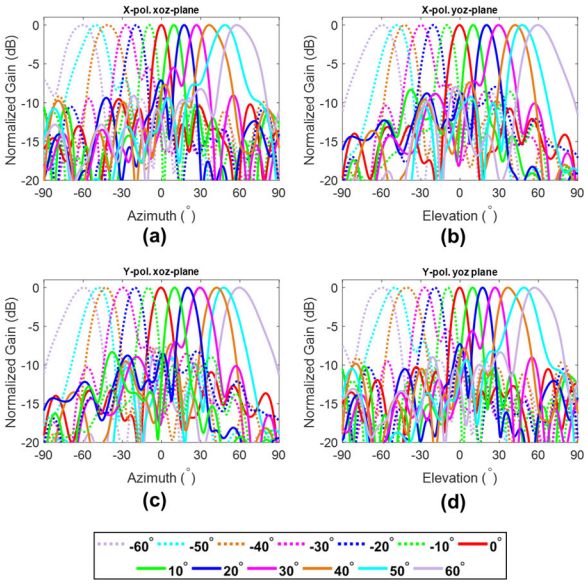

FIGURE 11. Simulated normalized radiation patterns for beam-steering under *x*-polarized incidence in (a) the azimuth plane (*xoz*-plane) and (b) the elevation plane (*yoz*-plane), and under *y*-polarized incidences in (c) azimuth plane and (d) elevation plane.

Usually at large beam-steering angles, the RRA may generate degraded radiation patterns with higher side lobe levels (SLLs) and distorted main lobes. Despite the effects from the feeding antenna, 3D printed supporter, coaxial cable blockages, and fabrication accuracy, the measured SLLs at broadside beam directions are less than −10 dB for both orthogonal polarizations and both observation planes. These issues are primarily attributed to the small aperture size and the impact of oblique incidence on the unit cell. An RRA with a larger aperture may be considered to reduce the SLL, and enhancing the quantization of bit numbers can lead to improved radiation performance as demonstrated

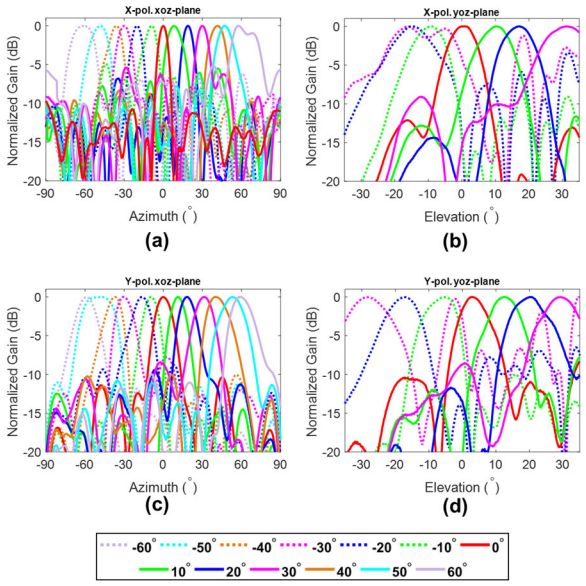

FIGURE 12. Measured normalized radiation patterns for beam-steering under *x*-polarized incidence in (a) the azimuth plane (*xoz*-plane) and (b) the elevation plane (*yoz*-plane), and under *y*-polarized incidence in (c) azimuth plane and (d) elevation plane.

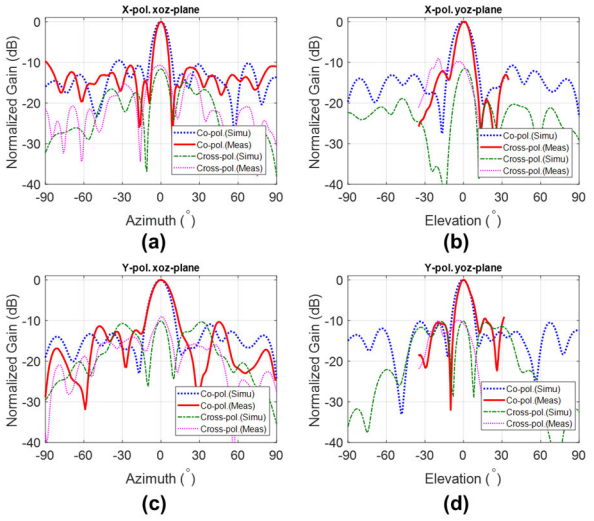

FIGURE 13. Comparison of broadside beams for co- and cross-polarizations under *x*-polarized incidence in (a) *xoz*-plane and (b) *yoz*-plane, and under *y*-polarized incidence in (c) *xoz*-plane and (d) *yoz*-plane.

in [31]. In the simulation, the half-power beam widths (HPBWs) exhibit an increasing trend as the beam steering direction deviates from the broadside position, with the HPBWs reaching a maximum of 23.26° at a beam-steering angle of 60°. For both orthogonal polarizations and both observation planes, the average HPBW at the broadside beam is 11.82°. While the HPBW of measured results reach up to 24°. The measured results closely match the simulated ones, particularly in the main beam's region. The average value of measured HPBW at the broadside beam direction is 10.75°, which is in good agreement with simulated ones. Therefore, these measured results validate simulations, verifying that the proposed RRA can achieve efficient and precise beam-steering performance. This further indicates a variety of applications, including wireless communications and radar systems. The inherent flexibility and adaptability of the RRA present novel prospects for improving antenna performance and system functionality.

Figure 13 displays the co- and cross-polarizations when a *y*-polarized wave is incident in the broadside beam direction. The cross-polarization level (CPL) is observed to be approximately less than −10 dB. These results demonstrate that the proposed RRA exhibits acceptable polarization independence for dual-polarization beam-steering. To improve this performance, modifications could be made to the unit cell to minimize cross-polarization reflections and an offset feed design could be used to minimize the effect of scattered fields from the feed antenna. The comparison of RRA's gain and aperture efficiency (AE) as a function of beam-steering angle for both the *x*- and *y*-polarized incidences on both the azimuth and elevation planes are plotted in Figure 14. Despite some gain and AE discrepancy between simulations and measurements, the gain of the main lobe remains stable, with a maximum reduction in gain of approximately 3 dB within the scanning range, indicating better beam scanning performance in both planes. Furthermore, a slight difference in the gain as a function of beam-steering is observed between the simulated and measured results. In addition, the measured maximum gains are 13.9 dBi and 12.9 dBi under *x*- and *y*-polarizations which correspond to the AE of about 9.1% and 7.4%, respectively. Besides, in simulations, the maximum gains are 15.4 dBi and 14.7 dBi and the corresponding AEs are around 12.8% and 10.9%, respectively. The difference between simulation and measurement results can be explained by the following reasons. First, the RLC equivalent circuit model used to describe the PIN diode properties in the simulation model may differ from the real PIN diode properties. In simulations, we use an equivalent model based on the datasheet, which does not consider the coupling effect between PIN diodes and physical structures. Second, the dimensions of the feeding source in simulations are retrieved from the official datasheet, which may differ from the real product. Also, prototype installation, assembly and alignment may cause errors in the measurement setup and measurement accuracy. In addition, it may be caused by fabrication tolerances and soldering errors in the prototype manufacturing process. However, the measured and simulated results remain consistent in terms of the overall performance trends exhibited by typical RRAs.

Table 1 compares the beam-steering capabilities of the proposed RRA to other existing works published in literature on 1-bit RRA based on PIN diodes. The beam-steering range of the proposed RRA is ±60°, which is similar to [10] and [23], but wider than [5], [6], [22], [25]. The proposed RRA has an average SSL below −10 dB at the broadside for both orthogonal polarizations in both planes, which

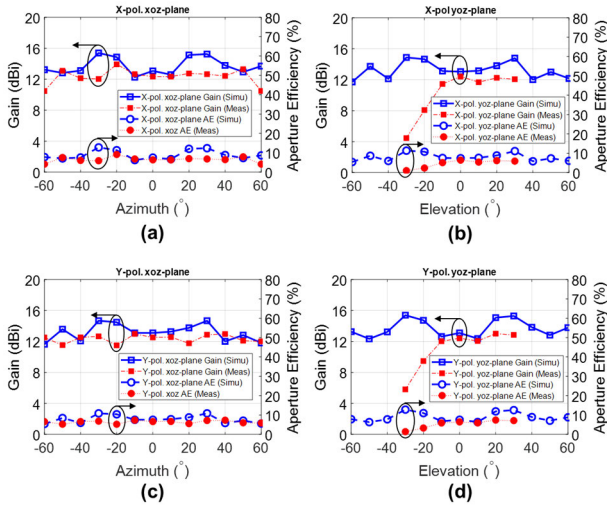

FIGURE 14. Maximum gain and aperture efficiency as a function of beam-steering angle under *x*-polarized incidence in (a) *xoz*-plane (b) and *yoz*-plane, and under *y*-polarized incidence in (c) *xoz*-plane and (d) *yoz*-plane.

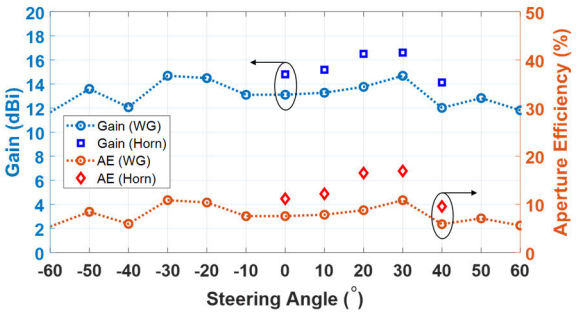

FIGURE 15. Comparison of gain and aperture efficiency between open-ended waveguide and horn antenna as the feeding antenna under *y*-polarized incidence in the azimuth plane.

TABLE 1. Comparison of 1-bit RRAs based on PIN diodes as tuning devices.

Ref.	RRA's size	Center Freq. (GHz)	Max. Beam	AE	SSL (dB)
[5]	12 × 12	5	± 50°	15.3%	−10
[6]	12 × 12	5.8	± 45°	14.9%	−8
[10]	14 × 14	12.5	± 60°	13.2%	−10
[11]	16 × 16	12.5	± 50°	15.4%	−10*
[12]	16 × 16	15	± 60°	25%	−10
[22]	12 × 12	10.1	± 50°	20.3%	−10.8
[23]	16 × 16	10	± 60°	13.8%	−12
[25]	20 × 20	7.45	± 40°	16.4% (x-pol.) 15.5% (y-pol.)	−11
This work	**16 × 16**	**5.8**	**± 60°**	**9.1%** (x-pol.) **7.4%** (y-pol.)	**−10.9**

* Estimated from the figure in the article, AE: aperture efficiency, SLL: side lobe level

corresponds closely to the performance reported in previous studies [5], [6], [10], [11], [12], [22], [25]. Considering the AE of the RRA, the proposed work achieves a maximum measured AE when utilizing an open-ended waveguide under illuminations of *x*- and *y*-polarized incidences as 7.9% and 7.4%, respectively. This values are observed to be lower than those reported in existing works [5], [6], [10], [11], [12], [22], [23], [25], which is primarily due to the relatively low gain of the open-ended waveguide. As we know in the context of the RRA, the gain of the feeding antenna and its location play a crucial role in maximizing the AE of the RRA. Therefore, integrating a higher gain feeding antenna offers a substantial enhancement in the AE. In this particular work, a low-gain (∼8 dBi) open-ended waveguide is utilized as the feeding antenna to create a low-profile and low-feeding blockage RRA. On the other hand, other studies [5], [6], [11], [23] have used high-gain horn antennas (≥ 11 dBi) instead. The choice of the feeding antenna's gain leads to the differences in the AE of RRA. To confirm this, the proposed RRA is examined through simulations when illuminated by a horn antenna under *y*-polarizations in the azimuth plane, and its antenna gain and AE are compared with the case of open-ended waveguide, as shown in Figure 15. It is clearly observed that, at +30° beam-steering angles when RRA is illuminated by the horn antenna, the gain and AE are improved from 14.68 dB to 16.61 dB (1.93 dB improvement) and from 10.9% to 16.9% (6% improvement), respectively. It is shown that the AE of the proposed RRA is similar to [25] and higher than [5], [6], [11], [23] which are illuminated by a horn antenna. This comparative analysis will help determine the impact of the feeding antenna's gain on the overall efficiency and performance of the RRA.

The proposed RRA offers valuable versatility and precision in beamforming applications, making it a valuable tool in radar and communication systems. In monopulse radar systems, generating sum and difference beams typically requires complex hardware, but with an RRA, this can be achieved directly using a simplified mechanism [32], [33], [34]. In different beams, a null point is desired at the midpoint, which can be achieved through phase cancellations between multiple beams. By adjusting the phases, specific radiation patterns can be created, which is particularly useful in monopulse radar systems for accurate target angle measurements and tracking. To illustrate this functionality of the proposed RRA, digital phase coding schemes are assigned to each unit cell of RRA, as depicted in Figure 16(a). In Figure 16(b), it is observed through simulations that the

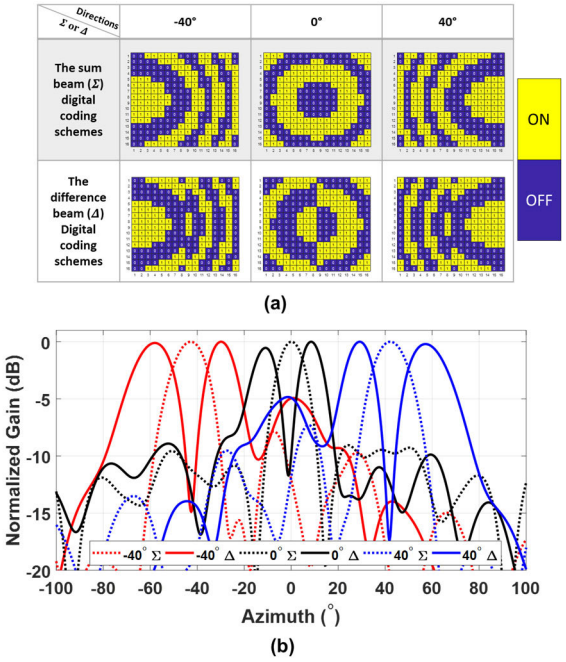

FIGURE 16. Sum and difference beams generated by the proposed RRA. (a) Phase distribution coding scheme (yellow: on-state, blue: off-state). (b) Radiation patterns.

radiation patterns for both sum and difference beams exhibit the ability to steer at the broadside with $\pm 40^\circ$ angles.

V. CONCLUSION

In this work, a metasurface-based 1-bit electronically reconfigurable reflectarray antenna (RRA) for dual-polarization beam-steering is proposed. The RRA is composed of 16×16 novel Jerusalem cross-shaped unit cells, each of which is loaded with two PIN diodes that enable a reflection phase switching of 180° between the diode states. The RRA is designed, fabricated, and measured along with the DC bias network, the shift registers based on a programmable control board, and a microcontroller. A standard open-ended waveguide is used as a feeding antenna, which is placed at an optimum feeding location of $f/D = 0.5$. The performance of the proposed RRA is achieved with dual-polarized beam-steering of up to $\pm 60^\circ$ in both azimuth and elevation planes. Furthermore, the aperture efficiency can be improved by using a high-gain feeding antenna. Additionally, the proposed RRA can be utilized to generate sum and difference beams for monopluse radar systems, which is confirmed by simulations. It is anticipated that the proposed RRA has the potential to be used in wireless communications, radar, and imaging systems.

ACKNOWLEDGMENT

The authors thank the Wireless Communication Research Laboratory, Electronics and Telecommunication Engineering Department, Rajamangala University of Technology Thanyaburi (RMUTT), Thailand, for providing measurement facilities and anechoic chamber.

REFERENCES

[1] K. Iqbal and Q. U. Khan, "Review of metasurfaces through unit cell design and numerical extraction of parameters and their applications in antennas," *IEEE Access*, vol. 10, pp. 112368–112391, 2022.
[2] S. Zahra, L. Ma, W. Wang, J. Li, D. Chen, Y. Liu, Y. Zhou, N. Li, Y. Huang, and G. Wen, "Electromagnetic metasurfaces and reconfigurable metasurfaces: A review," *Frontiers Phys.*, vol. 8, Jan. 2021, Art. no. 593411.
[3] B. Rana, S.-S. Cho, and I.-P. Hong, "Review paper on hardware of reconfigurable intelligent surfaces," *IEEE Access*, vol. 11, pp. 29614–29634, 2023.
[4] H. D. Cuong, M.-T. Le, N. Q. Dinh, X. N. Tran, and N. Michishita, "A broadband 1-bit single-layer reconfigurable reflectarray unit cell based on PIN diode model," *IEEE Access*, vol. 11, pp. 6477–6489, 2023.
[5] J. Han, L. Li, G. Liu, Z. Wu, and Y. Shi, "A wideband 1 bit 12×12 reconfigurable beam-scanning reflectarray: Design, fabrication, and measurement," *IEEE Antennas Wireless Propag. Lett.*, vol. 18, no. 6, pp. 1268–1272, Jun. 2019.
[6] W. Luo, S. Yu, N. Kou, Z. Ding, and Z. Zhang, "An electronically 1-bit reconfigurable beam-steering reflectarray antenna of 12×12 units integrated with PIN diodes," *Prog. Electromagn. Res. Lett.*, vol. 104, pp. 7–13, 2022.
[7] S.-G. Lee, Y.-H. Nam, Y. Kim, J. Kim, and J.-H. Lee, "A wide-angle and high-efficiency reconfigurable reflectarray antenna based on a miniaturized radiating element," *IEEE Access*, vol. 10, pp. 103223–103229, 2022.
[8] B. J. Xiang, X. Dai, and K.-M. Luk, "A wideband low-cost reconfigurable reflectarray antenna with 1-Bit resolution," *IEEE Trans. Antennas Propag.*, vol. 70, no. 9, pp. 7439–7447, Sep. 2022.
[9] H. Yang, F. Yang, X. Cao, S. Xu, J. Gao, X. Chen, M. Li, and T. Li, "A 1600-element dual-frequency electronically reconfigurable reflectarray at X/Ku-band," *IEEE Trans. Antennas Propag.*, vol. 65, no. 6, pp. 3024–3032, Jun. 2017.
[10] Z. Wang, Y. Ge, J. Pu, X. Chen, G. Li, Y. Wang, K. Liu, H. Zhang, and Z. Chen, "1 bit electronically reconfigurable folded reflectarray antenna based on p-i-n diodes for wide-angle beam-scanning applications," *IEEE Trans. Antennas Propag.*, vol. 68, no. 9, pp. 6806–6810, Sep. 2020.
[11] B. Xi, Y. Xiao, K. Zhu, Y. Liu, H. Sun, and Z. Chen, "1-bit wideband reconfigurable reflectarray design in Ku-band," *IEEE Access*, vol. 10, pp. 4340–4348, 2022.
[12] S.-G. Zhou, G. Zhao, H. Xu, C.-W. Luo, J.-Q. Sun, G.-T. Chen, and Y.-C. Jiao, "A wideband 1-bit reconfigurable reflectarray antenna at Ku-band," *IEEE Antennas Wireless Propag. Lett.*, vol. 21, no. 3, pp. 566–570, Mar. 2022.
[13] H. Li, X. Qi, T. Zhou, Z. Xu, and T. A. Denidni, "Wideband reconfigurable reflectarray based on reflector-backed second-order bandpass frequency selective surface," *IEEE Trans. Antennas Propag.*, vol. 70, no. 12, pp. 12334–12339, Dec. 2022.
[14] X. Yang, S. Xu, F. Yang, M. Li, Y. Hou, S. Jiang, and L. Liu, "A broadband high-efficiency reconfigurable reflectarray antenna using mechanically rotational elements," *IEEE Trans. Antennas Propag.*, vol. 65, no. 8, pp. 3959–3966, Aug. 2017.
[15] A. J. Rubio, A.-S. Kaddour, and S. V. Georgakopoulos, "A mechanically rollable reflectarray with beam-scanning capabilities," *IEEE Open J. Antennas Propag.*, vol. 3, pp. 1180–1190, 2022.
[16] X. Liu, L. Schmitt, B. Sievert, J. Lipka, C. Geng, K. Kolpatzeck, D. Erni, A. Rennings, J. C. Balzer, M. Hoffmann, and A. Czylwik, "Terahertz beam steering using a MEMS-based reflectarray configured by a genetic algorithm," *IEEE Access*, vol. 10, pp. 84458–84472, 2022.
[17] X. Li, H. Sato, Y. Shibata, T. Ishinabe, H. Fujikake, and Q. Chen, "Development of beam steerable reflectarray with liquid crystal for both E-plane and H-plane," *IEEE Access*, vol. 10, pp. 26177–26185, 2022.
[18] P. Aghabeyki, Y. Cai, G. Deng, Z.-H. Tan, and S. Zhang, "A dual-polarized reconfigurable reflectarray with a thin liquid crystal layer and 2-D beam scanning," *IEEE Trans. Antennas Propag.*, vol. 71, no. 4, pp. 3282–3293, Apr. 2023.
[19] P. I. Theoharis, R. Raad, F. Tubbal, M. U. A. Khan, and A. Jamalipour, "Wideband reflectarrays for 5G/6G: A survey," *IEEE Open J. Antennas Propag.*, vol. 3, pp. 871–901, 2022.
[20] P. Nayeri, F. Yang, and A. Z. Elsherbeni, "Beam-scanning reflectarray antennas: A technical overview and state of the art," *IEEE Antennas Propag. Mag.*, vol. 57, no. 4, pp. 32–47, Aug. 2015.
[21] H. Zhang, X. Chen, Z. Wang, Y. Ge, and J. Pu, "A 1-bit electronically reconfigurable reflectarray antenna in X band," *IEEE Access*, vol. 7, pp. 66567–66575, 2019.

[22] K. Zheng, K. Xu, S. Chen, T. Zhou, X. Pan, C. Zhang, and X. Yu, "One-bit wideband reconfigurable reflectarray with stable beam-scanning gain for X-band application," *Microw. Opt. Technol. Lett.*, vol. 65, no. 8, pp. 2323–2330, Aug. 2023.
[23] H. Luyen, Z. Zhang, J. H. Booske, and N. Behdad, "Wideband, beam-steerable reflectarray antennas exploiting electronically reconfigurable polarization-rotating phase shifters," *IEEE Trans. Antennas Propag.*, vol. 70, no. 6, pp. 4414–4425, Jun. 2022.
[24] H. Xu, S. Xu, F. Yang, and M. Li, "Design and experiment of a dual-band 1 bit reconfigurable reflectarray antenna with independent large-angle beam scanning capability," *IEEE Antennas Wireless Propag. Lett.*, vol. 19, no. 11, pp. 1896–1900, Nov. 2020.
[25] N. Zhang, K. Chen, J. Zhao, Q. Hu, K. Tang, J. Zhao, T. Jiang, and Y. Feng, "A dual-polarized reconfigurable reflectarray antenna based on dual-channel programmable metasurface," *IEEE Trans. Antennas Propag.*, vol. 70, no. 9, pp. 7403–7412, Sep. 2022.
[26] S.-G. Lee and J.-H. Lee, "A dual-polarized reconfigurable reflectarray antenna based on a symmetrically rotated sub-array," *IEEE Access*, vol. 11, pp. 55657–55663, 2023.
[27] M. Wang, Y. Mo, W. Xie, N. Hu, Z. Chen, and Z. Tian, "A 1-bit all-metal wide-angle and multipolarization beam-scanning reconfigurable reflectarray antenna," *IEEE Antennas Wireless Propag. Lett.*, vol. 22, no. 5, pp. 1015–1019, May 2023.
[28] G.-B. Wu, S.-W. Qu, S. Yang, and C. H. Chan, "Broadband, single-layer dual circularly polarized reflectarrays with linearly polarized feed," *IEEE Trans. Antennas Propag.*, vol. 64, no. 10, pp. 4235–4241, Oct. 2016.
[29] M. H. Dahri, M. H. Jamaluddin, F. C. Seman, M. I. Abbasi, N. F. Sallehuddin, A. Y. I. Ashyap, and M. R. Kamarudin, "Aspects of efficiency enhancement in reflectarrays with analytical investigation and accurate measurement," *Electronics*, vol. 9, no. 11, p. 1887, Nov. 2020.
[30] M. Yi, Y. Bae, S. Yoo, and J. So, "Digitized reconfigurable metal reflectarray surfaces for millimeter-wave beam-engineering," *Appl. Sci.*, vol. 11, no. 13, p. 5811, Jun. 2021.
[31] H. Yang, F. Yang, S. Xu, M. Li, X. Cao, J. Gao, and Y. Zheng, "A study of phase quantization effects for reconfigurable reflectarray antennas," *IEEE Antennas Wireless Propag. Lett.*, vol. 16, pp. 302–305, 2017.
[32] X. Ma, J. Han, G. Li, M. Chang, Y. Tian, S. Chen, H. Liu, L. Li, and T. J. Cui, "A wideband 1-bit reconfigurable electromagnetic surface for monopulse radar applications," *IEEE Trans. Antennas Propag.*, vol. 71, no. 6, pp. 5475–5480, Jun. 2023.
[33] X. Pan, F. Yang, S. Xu, and M. Li, "A 10 240-element reconfigurable reflectarray with fast steerable monopulse patterns," *IEEE Trans. Antennas Propag.*, vol. 69, no. 1, pp. 173–181, Jan. 2021.
[34] X. Wan, Q. Xiao, Y. Z. Zhang, Y. Li, J. Eisenbeis, J. W. Wang, Z. A. Huang, H. X. Liu, T. Zwick, and T. J. Cui, "Reconfigurable sum and difference beams based on a binary programmable metasurface," *IEEE Antennas Wireless Propag. Lett.*, vol. 20, no. 3, pp. 381–385, Mar. 2021.

PUBET SANGMAHAMAD received the B.Eng. degree (Hons.) in electronics and telecommunication engineering from the Rajamangala University of Technology Thanyaburi (RMUTT), Thailand, in 2013, and the M.Eng. degree in electrical engineering from Srinakharinwirot University (SWU), Thailand, in 2018. He is currently pursuing the Ph.D. degree in electrical engineering with Chulalongkorn University (CU), Thailand. His research interests include metamaterials, metasurface, reflectarray antennas, and antenna technology.

PANUWAT JANPUGDEE (Member, IEEE) received the B.E. degree (Hons.) in electrical engineering from Chulalongkorn University, Thailand, and the M.S. and Ph.D. degrees in electrical engineering from The Ohio State University, USA. He is currently an Assistant Professor with the Department of Electrical Engineering, Chulalongkorn University. He has extensive experience in the uniform geometrical theory of diffraction (UTD) and its applications to radiation and scattering problems. His research interests include antennas, computational electromagnetics, and microwave engineering. He has also had some experience in the industry. He is a Founding Member of the Innovative Electromagnetic Academic of Thailand (iEMAT). He was the Vice Chair of the IEEE MTT/AP/ED Joint Chapter, Thailand Section. He has been a Reviewer of IEEE TRANSACTIONS ON ANTENNAS AND PROPAGATION, IEEE ANTENNAS AND WIRELESS PROPAGATION LETTERS, and *IET Microwave, Antennas and Propagation*.

YAN ZHAO (Senior Member, IEEE) received the B.Sc. degree from the Beijing University of Posts and Telecommunications (BUPT), China, the M.Sc. degree from the University of Birmingham, U.K., and the Ph.D. degree from the Queen Mary University of London, U.K. Currently, he is a Professor of electrical engineering with Chulalongkorn University, Thailand. He has published over 100 technical papers in highly-ranked journals and refereed conference proceedings. He has extensive experience in computational electromagnetics, notably in the area of finite-difference time-domain (FDTD) methods for metamaterials. He also has experience in the ray tracing technique, the uniform theory of diffraction (UTD), and their applications in antenna engineering and radio propagation. He is a Founding Member of the Innovative Electromagnetic Academic of Thailand (iEMAT) and the Managing Editor of *Engineering Journal*. He was the Chair of the IEEE Thailand Section Joint MTT/APS Chapter. He has served as a Regular Reviewer for IEEE TRANSACTIONS ON ANTENNAS AND PROPAGATIONS, IEEE ANTENNAS AND WIRELESS PROPAGATION LETTERS, IEEE MICROWAVE AND WIRELESS COMPONENTS LETTERS, *Progress in Electromagnetics Research*, and *Optics Express*.